Wider is Better? Contact-free Vibration Sensing via Different COTS-RF Technologies

Zhe Chen[†], Tianyue Zheng[‡], Chao Cai[§], Yue Gao[¶], Pengfei Hu[*], Jun Luo[‡],
[†] AIWiSe, China-Singapore International Joint Research Institute, China
[‡] Nanyang Technological University, Singapore
[§] Huazhong University of Science and Technology, China
[¶] Fudan University, China [*] Shandong University, China
Email: chenz@csijri.com, {tianyue002, junluo}@ntu.edu.sg, chriscai@hust.edu.cn, yue.gao@ieee.org, phu@sdu.edu.cn

***Abstract*—Vibration sensing is crucial to human life and work, as vibrations indicate the status of their respective sources (e.g., heartbeat to human health condition). Given the inconvenience of *contact sensing*, both academia and industry have been intensively exploring *contact-free vibration sensing*, with several major developments leveraging radio-frequency (RF) technologies made very recently. However, a measurement study systematically comparing these options is still missing. In this paper, we choose to evaluate five representative commercial off-the-shelf (COTS) RF technologies with different carrier frequencies, bandwidths, and waveform designs. We first unify the sensing data format and processing pipeline, and also propose a novel metric v-SNR to quantify sensing quality. Then our extensive evaluations start from controlled experiments for benchmarking, followed by investigations on two real-world applications: machinery vibration measurement and vital sign monitoring. Our comprehensive study reveals that Wi-Fi performs the worst among all five technologies, while a lesser-known UWB-based technology achieves the best overall performance, and others have respective pros and cons in different scenarios.**

***Index Terms*—Vibration sensing, contact-free sensing, RF sensing, COTS RF technologies, IR-UWB, mmWave radar.**

I. Introduction

Vibration takes place everywhere and all the time in our daily life and work [1]. Our human bodies vibrate as we have heartbeat and respiration, while our appliances and tools also vibrate as they may rotate (e.g., a fan) or reciprocate (e.g., a piston). These major vibrations, along with other accompanying vibrations (e.g., caused by friction or other types of resistance), strongly indicate the status of either a human body or a working part. For example, abnormal heartbeats proceed sudden cardiac attack [2], [3], and high vibrations of a wind turbine indicate its eccentric unbalances [4]. Therefore, *vibration sensing* has long been a crucial functionality that we heavily rely on. Conventional approaches to sensing vibration largely rely on *contact sensors* that directly touch the target object [5]. Though these approaches certainly produce accurate results, the contact nature can be inconvenient (e.g., for people) or even impractical (e.g., for rotational parts). Consequently, *contact-free sensing* has been a research target for both academia [6], [7], [8], [9], [10] and industry [11], [12] in the past several decades.

[*] Corresponding author: Pengfei Hu, Shandong University, China

Among all the existing contact-free sensing methodologies, two major developments on radio-frequency (RF) sensing have taken place in the last couple of years. On one hand, several commercial off-the-shelf (COTS) radios have been produced by major electronics manufacturers [13], [14], [15], [16]; they offer a wide choice in terms of the operating frequency, ranging from 7 to 77 GHz. On the other hand, research communities have gained a deeper understanding of Wi-Fi sensing [17], thus more effectively exploiting this communication infrastructure for sensing purpose. In fact, academic researchers have started using these COTS radios for various vibration sensing purposes, which include, among others, millimeter-Wave (mmWave) radios and Impulse-Radio Ultra WideBand (IR-UWB) for human vital sign monitoring [18], [9], [19], and mmWave radios for human speech sensing (lip or vocal folds vibrations) [20], [21]. Given all these mature technologies and potential applications, a question naturally arising when facing a certain application is: *which technology performs the best for contact-free vibration sensing?*

A closely related measurement study has partially answered the above question, focusing only on monitoring respiratory rate during sleep [22]. However, our study delivers novel insights in the following five aspects. First, we propose a new metric, v-SNR, to quantify general RF vibration quality. Second, we evaluate only mature RF sensing technologies. This substantially increases the applicability of our study results, while enabling us to perform the study using a unified processing pipeline. Third, we consider general vibration sensing and hence a broader range of applications. As these applications share the vibration nature but vary in, e.g., frequency and strength, putting them side-by-side allows us to better understand the capability of individual RF sensing technologies. Fourth, we consider sensing applications in real-life settings, very different from the single fixed experiment scenario in [22]. This makes our study more realistic as, in practice, RF sensing has to be performed under uncertain conditions, e.g., various distances or even non-line-of-sight (NLOS). Finally, we examine the ability of multi-target monitoring often demanded by real-life applications.

Essentially, we consider five RF technologies, namely Wi-Fi at 5 GHz, IR-UWB at 7 GHz [13], and (near-)mmWave radios

at 24, 60, and 77 GHz [14], [15], [16]. These technologies all process received signals in a joint time-frequency manner, enabling us to unify existing proposals (e.g., [8], [18]) with a general sensing model and processing pipeline. We take a LEGO rotary as the base application to provide micro-benchmarks for all five technologies, aiming to understand their pros and cons under various conditions. In addition, we perform case studies on both machinery vibration sensing and human respiration/heartbeat monitoring. Different from the clinical study with fixed settings in [22], our study on vital sign monitoring is conducted under daily-life environments, mimicking realistic healthcare applications. The following major contributions and insights are made and drawn from our extensive experiments:

- We propose a general metric, v-SNR, to quantify general RF vibration sensing quality; such a widely applicable metric has never appeared in literature.
- Wi-Fi, as a communication-oriented device, is far from useful for vibration sensing.
- mmWave radios, though highly boosted by industry and performing reasonably well, are not cost-effective.
- Lesser-used IR-UWB and 24 GHz mmWave radio can have the best overall performance.
- Leveraging to v-SNR, we we provide the guidelines for vibration measurements with different RF technologies.

The rest of this paper is organized as follows: Sec. II briefly studies the literature on mechanical and human-centered vibration sensing. Sec. III presents the generic model of the RF vibration sensing, which in turn allows us to introduce the novel metric v-SNR. Sec. IV shows the data pre-processing and sensing algorithms in our paper. Sec. V elaborates on the evaluation results under various realistic settings. Sec. VI concludes our paper.

II. Related Work

RF vibrometry has been recently applied to both mechanical vibration measurement and vital sign monitoring, and a comparative study on RF respiratory monitoring has also been reported in [22]. However, [22] solely focuses on *multistatic* devices, whereas we devote our study to *monostatic* ones. For example, their *multistatic* IR-UWB is a communication-oriented device with a separated transmitter (tx)-receiver (rx) pair, while our *monostatic* IR-UWB with a single transceiver is a COTS device dedicated to sensing. Therefore, we exclude proposals discussed in [22], but include multistatic Wi-Fi in our study for backward compatibility.

A. Mechanical Vibration Measurement

Early proposals employ specially designed hardware as RF vibrometry for robots [23] and actuators [24]. Wi-Fi device for vibrometry [25] emerge later due to its reliance on commercial hardware. Recent years have witnessed a revival of RF technologies with a large bandwidth, including IR-UWB [26] and mmWave radars [27], with the latest RF vibrometry achieving micrometer-level precision [8]. Meanwhile, audio sensing that aims to recover acoustic signal by sensing vibrations produced by speakers [28] or human voice cords [20], [21] becomes a research hotspot. As for the algorithm, Fourier transform is enough for general vibrometry [26], [24], [27], [28], while advanced learning technique [20] and mode decomposition algorithm [21] may be needed for more complex tasks such as audio sensing.

B. Vital Sign Monitoring

Applying RF vibrometry to clinical scenarios or even domestic environments leads to vital sign monitoring. Similar to the general vibration sensing, Wi-Fi was firstly adopted to estimate respiratory rate [29], [30] and heart rate [31] due to its wide availability. Though some researches still stick to Wi-Fi sensing [32], dedicated COTS devices have been increasingly considered, including IR-UWB monitoring for respiration [18], [19] and heartbeat [33], [18], as well as mmWave radars monitoring for the same purposes [24], [27]; both IR-UWB and mmWave radars have capacity to handle multiple users [18], [34].

Apart from the hardware differences, differences of vital sign estimation algorithms should also be noted. The traditional method for estimating vital sign frequencies is non-parametric Fourier transform [31]; to counter the lack of precision and reliability of Fourier transform, parametric autoregressive [35] and state space method [36] are also used. Moreover, due to the non-stationarity of vital signals, mode decomposition methods have also been explored to break down the signal. Examples include empirical mode decomposition [37], ensemble empirical mode decomposition [38] and variational mode decomposition [18].

III. Common RF Sensing Model

In this section, we first introduce a common model for characterizing the impact of vibration on an RF channel, then we explain how individual RF technologies respond to (thus sense) the vibration.

A. Vibration RF Channel Model

Given a pair of transmitter and receiver, in an indoor environment with P propagation paths, we model the baseband RF channel as follows [39]:

$$h(t) = \sum_{p=1}^{P} \alpha_p e^{j2\pi f_c \tau_p} + n(t), \tag{1}$$

where f_c is the carrier frequency, α_p is the amplitude of p-th path, and $n(t)$ is Gaussian noise with variance σ^2. In particular, we have $\tau_p = \tau_p^s + \tau_p^v$ where τ_p^s and τ_p^v are the p-th time delays caused by static reflections and vibration reflections, respectively. Though $\tau_p^s = d_p/c$ with d_p being the path length and c being the light speed, τ_p^v is far more complicated. We follow the convention to describe any vibration via a spinning geometric model [25], [40]. Defining *vibration radius* r as the distance between spinning center and the reflector point, we model the displacement as:

$$\Delta d_p(t) \approx r\left[1 - \cos\left(2\pi f_p^v t\right)\right], \tag{2}$$

where f_p^v is the vibration frequency of the p-th path. This allows us to compute $\tau_p^v(t)$ as $\Delta d_p(t)/c$.

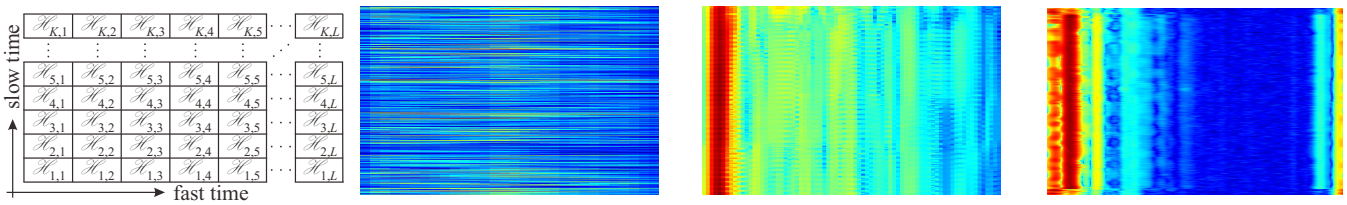

(a) RF signal matrix $\mathscr{H}$. (b) Wi-Fi matrix. (c) IR-UWB matrix. (d) FMCW matrix.

Fig. 1: The RF signal matrix and corresponding vibration sensing heatmaps for three RF techniques. Multiple vibrations at different distances can be clearly seen from the fast-time *bin*s in both (c) and (d).

Considering a transmitted signal $s(t)$, the received signal is $y(t) = h(t) * s(t)$, where $*$ denotes convolution. Although the *vibration reflection time delay* $\tau_p^{\mathrm{v}}(t)$ contained in $y(t)$ is always used to sense a vibration, individual technologies may differ significantly due to their distinct features (see Table I for those involved in our study), yet we intend to unify them into a common framework in the following. For the sake of brevity, we hereby consider only one path (thus removing the subscript p), and omit the noise term.

TABLE I: The list of COTS RF sensing devices: FoV comprises two angles, namely *azimuth* and *elevation*.

RF techs	Devices	Freq (GHz)	BW (GHz)	FoV (Degree)
Wi-Fi	Intel 5300 [17]	2.4, 5.8	0.04	360,90
IR-UWB	Novelda X4 [13]	7.29	1.4	120,120
mmWave	Infineon XENSIV [14]	24	0.25	76,19
mmWave	TI IWR6843 [15]	60	4	120,120
mmWave	TI IWR1443 [16]	77	4	56,28

B. Wi-Fi

As Wi-Fi adopts Orthogonal Frequency Division Multiplexing (OFDM), we use L, e_ℓ, and y_ℓ^W to denote the number of OFDM subcarriers, the ℓ-th subcarrier, and the received signal, respectively. Then, we have

$$y_\ell^{\mathrm{W}}(t) = \alpha_\ell e^{j2\pi f_\ell \phi(t)} s_\ell, \quad \ell \in \{1, ..., L\}, \tag{3}$$

where α_ℓ is the channel gain of ℓ-th subcarrier, f_ℓ is the frequency of the ℓ-th subcarrier, and $\phi(t) = [d + \Delta d(t)]/\mathrm{c}$. To obtain the *channel state information* (CSI) of Wi-Fi, the zero-forcing receiver is applied $\hat{h}_\ell = y_\ell^{\mathrm{W}}/s_\ell$. Since each CSI vector of a packet $[\hat{h}_\ell]_{\ell \in \{1,\cdots,L\}}$ has L OFDM subcarriers, K packets induce a $K \times L$ signal matrix. We define K as *slow-time* and L as *fast-time* because they sample the signal at different timescales. Figure 1(a) illustrates this signal model, and Figure 1(b) provides the vibration Wi-Fi matrix as an example. Due to the narrow bandwidth of Wi-Fi, its baseband signal offers a very coarse-grained resolution (e.g., 7.5 m with 40 MHz bandwidth) to differentiate d, so we have $d + \Delta d(t) \approx \Delta d(t)$, which we summarize as "having only one distance *bin* along the fast-time dimension". In other words, Wi-Fi is largely confined to sensing only one vibration target. Fortunately, $\Delta d(t)$ can still be sensed along the slow-time dimension leveraging the carrier phase and amplitude.

C. IR-UWB

Designed specifically for sensing purpose, an IR-UWB transmits pulses of extremely short time duration. Therefore, the baseband signal occupies a wide bandwidth B (usually $B \geq 1$ GHz), and thus offers a fine-grained resolution in the time domain. We can write the received pulse signal $y^{\mathrm{I}}(t)$ as:

$$y^{\mathrm{I}}(t) = \alpha e^{j2\pi f_{\mathrm{c}} \phi(t)} e^{-\frac{(t - T_{\mathrm{tx}}/2 - \phi(t))^2}{2\epsilon_{\mathrm{tx}}^2}}, \tag{4}$$

where $\epsilon_{\mathrm{tx}} = \frac{1}{2\pi B_{-10\ \mathrm{dB}} (\log_{10}(e))^{1/2}}$ is the standard deviation of the Gaussian pulse which determines the -10 dB bandwidth, and $T_{\mathrm{tx}} = 1/B$ is the signal duration, respectively. We gather L time-domain samples to form a fast-time vector: due to very short T_{tx}, each sample can be deemed as a *bin* corresponding to a certain value of the static distance d. We can stack K such L-dimensional vectors to build a $K \times L$ signal matrix. Essentially, each range bin contains a K-dimensional slow-time vector, whose phase and amplitude can be used to sense $\Delta d(t)$. The Figure 1(c) shows such an IR-UWB matrix. Different from Wi-Fi, IR-UWB can sense both d and $\Delta d(t)$ due to its much wider bandwidth (1.4GHz as shown in Table I); we shall leverage this to both monitor multiple vibration targets and also to remove background inferences.

D. mmWave Radio

Operating at a center frequency of several tens of GHz (24, 60, 77 GHz in Table I), mmWave radio is another dedicated COTS sensing technology. Typically, a mmWave radio exploits Frequency-Modulated Continuous-Wave (FMCW) to transmit a chirp signal that sweeps across a wide frequency spectrum. Denoting the total bandwidth by B and the time span of a single chirp by T^{S}, it is shown in [41] that the reflected signal $y^{\mathrm{M}}(t)$ can be written as:

$$y^{\mathrm{M}}(t) = \alpha V_{\mathrm{tx}} \Pi\left(t - \phi(t)\right) e^{-j2\pi\left(\beta\phi(t)t + f_{\mathrm{c}}\phi(t) - \beta\phi^2(t)/2\right)}, \tag{5}$$

where $\beta = B/T^{\mathrm{S}}$, V_{tx} is the amplitude of the transmitted signal and $\Pi(t)$ is a rectangular function with range $[-T^{\mathrm{S}}/2, T^{\mathrm{S}}/2]$. Time-domain sample of the signal given by Eqn. (5) forms an L-dimensional vector, where the frequency $\beta\phi(t)$ and the phase $f_{\mathrm{c}}\phi(t) - \beta\phi^2(t)/2$ characterize how the signal changes over time. We further apply FFT to transform a vector into its frequency-domain, then we construct a $K \times L$ signal matrix by stacking K transformed vectors, as shown

in Figure 1(d). As these mmWave radios also occupy a wide bandwidth (often several GHz), each frequency sample in an L-dimensional fast-time vector can be deemed as a bin, so that frequency peaks can be exploited to differentiate static distances d. More importantly, since their carrier frequencies are much higher (up to 10 times of other RF technologies), the resulting very short wavelength yields a higher sensitivity to the vibration induced $\Delta d(t)$.

Remarks: Some of these RF technologies have multiple radio transceivers, so the signal matrix defined for all three RF technologies comes from only one tx-rx antenna pair. In the following, we shall focus on just one signal matrix, but adopt existing algorithm [22] to select the best antenna pair.

E. Vibration Sensing Quality: A New Perspective

Different from the signal-to-noise ratio (SNR) measured for both direct and reflection paths in communication, RF sensing always focuses on the reflection paths, and thus needs a new metric to quantify its performance. Consequently, we aim to define the vibration SNR (or v-SNR) to quantify general RF vibration sensing performance. Considering the limited bandwidth B in Sec. III, we can rewrite the Eqn. (1) in the following:

$$h(t) = \sum_{p=1}^{P} \alpha_p e^{-j2\pi f_c \phi_p(t)} \text{sinc}[2B(t - \phi_p(t))] + n(t), \quad (6)$$

where $\text{sinc}(t) = \frac{\sin t}{t}$ is the sampling function with limited bandwidth B. Recalling the $K \times L$ signal matrix shown in Fig. 1a, we have $t = k\Delta t + \ell K \Delta t$ where Δt is the slow-time frame period. Eqn. (6) yields two important insights for us: i) when the bandwidth B is very large, $\lim_{B\to+\infty} \text{sinc}(2Bt) = \delta(t)$, making the extraction of vibration signals more precise, and ii) B is also a crucial factor affecting on the physical separability of multiple vibration sources.

To verify our statements, we conduct experiments using four COTS RF sensing devices with different bandwidths. In our experiments, the two subjects vibrate with 49 and 90 rpm, respectively, and they are separated by a distance of 37.5 cm. We depict the heatmaps of the resulting signal matrix in Fig. 2. On one hand, Fig. 2a and 2b indicate that two vibration subjects are merged together, because the insufficient bandwidth of Wi-Fi and 24 GHz leads to a range resolution too low to separate the subjects. On the other hand, IR-UWB and 60 GHz have much finer-grained resolution due to their wider bandwidth, allowing them to clearly distinguish the two vibration subjects and also be more robust to noise and interference, as shown by Fig. 2c and 2d.

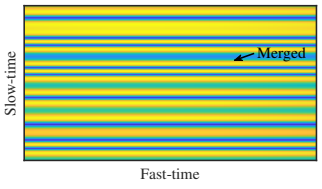

(a) Wi-Fi with 0.04 GHz bandwidth.

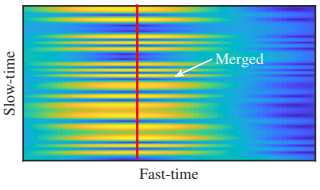

(b) 24 GHz with 0.25 GHz bandwidth.

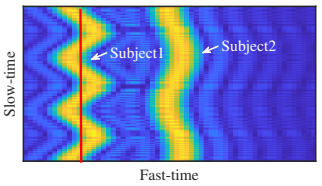

(c) IR-UWB with 1.4 GHz bandwidth.

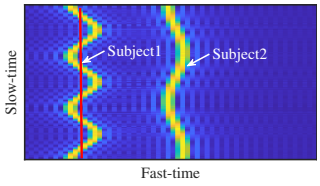

(d) 60 GHz with 4 GHz bandwidth.

Fig. 2: The signal matrix with different bandwidths B for sensing the vibrations of two subjects.

To quantify general RF vibration sensing quality, we derive the p-th reflection channel by $\hbar_p$ based on Eqn (6) as:

$$\hbar_p(k,\ell) = \alpha_p e^{-j2\pi f_c \phi_p(k,\ell)} \text{sinc}[2B(k\Delta t - \phi_p(k,\ell))]. \quad (7)$$

Let $p = n$ denote the vibration subject of interest and $p = m$ otherwise, we now define the v-SNR as follows:

$$\gamma_n(k,\ell) = 10 \log \left(\frac{|\hbar_n(k,\ell)|^2}{\sum_{m \in Q^{\text{I}}} |\hbar_m(k,\ell)|^2 + \sigma^2} \right), \quad (8)$$

where Q^{I} refers to the interfering reflection set.

Defined for a specific bin ℓ in Eqn. (8), v-SNR of a given subject should be the maximal one achieved among a set of bins around the actual range of the subject. However, Fig. 2 (apart from Fig. 2a) also reveals an interesting property of the signal matrix: because vibration may affect the range of the subject, a single bin may fail to capture the real vibration trace. As shown by the red vertical line indicating the maximal v-SNR bin for the first subject, it could even sample the noise (blue) region in Fig. 2d when the fine-grained range resolution leads to a very narrow vibration trace, resulting in invalid readings (especially in terms of phase). Therefore, while a wider bandwidth does improve the range resolution so that different subjects can be differentiated, it may potentially invalidate the bin-based sampling rule. Under such circumstance, we are left with two choices in practice: **either sampling vibration by strictly following its (curved) trace yet with very high complexity, or sticking to bin-based sampling but avoid using a too wider bandwidth.**

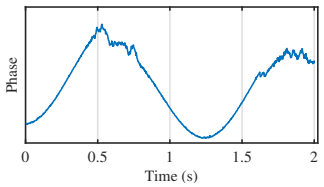

(a) Fast-time bin 1 (maximal).

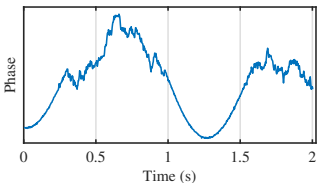

(b) Fast-time bin 2.

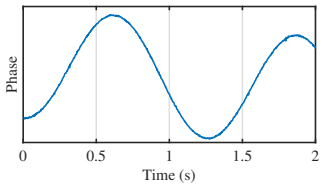

(c) Curved tracing.

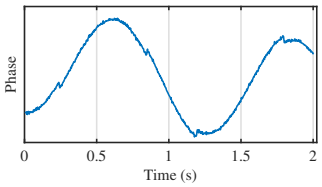

(d) Bin merging.

Fig. 3: Sampling vibration in 4 GHz bandwidth in different ways: (a) optimal bin-based, (b) sub-optimal bin-based, (c) (vibration) curve tracing, (d) bin merging with downsampling.

We also conduct the experiments using the 60 GHz radar to verify our statements. We first adopt the bin-based sampling and plot the phase changes of the optimal bin and sub-optimal bin in Fig. 3a and 3b, respectively. Apparently, phase noises are introduced due to bad sampling around the (amplitude) peak regions. Though sophisticated curve tracing obtains perfect phase readings in Fig. 3c, a simplified alternative merging a couple of close-by bins via downsampling also gain near-perfect outcome in Fig. 3d.

IV. Experiment Methodology

Different from pure respiration monitoring [22] where the vibration frequency is known to exist only within a very narrow range, general vibration sensing cannot assume such a strong prior. In addition, there might exist multiple vibration targets and even the same target may produce different vibration frequencies. Therefore, our vibration sensing methodology stresses on data pre-processing, as using the impact of $\Delta d(t)$ on the slow-time dimension to deduce a certain vibration frequency is rather standard.

A. Pre-processing

The signal matrix of any RF technology goes through the following pre-processing pipeline.

a) Static Clutter Suppression: A typical indoor environment always causes reflection signals from static objects (e.g., furniture and walls), beside the vibration targets. These static reflections can often be so strong to bury the vibration reflections. Therefore, suppressing such *static clutter*s is very important. Among many static clutter suppression approaches [41], we choose a simple yet efficient moving difference filter as these reflections remain invariant to $\Delta d(t)$. Essentially, we estimate the residue signal matrix $\mathscr{R}$ as:

$$\mathscr{R}(i,j) = \beta\left[\mathscr{H}(i,j) - \mathscr{R}(i,j-1)\right] \tag{9}$$

where i, j index fast-time and slow-time respectively, $\mathscr{H}(i,j)$ is an element of the signal matrix, $\beta \in (0.95, 1)$. The vibration induced reflections should be largely contained in $\mathscr{R}$.

b) Vibrating Target Differentiation: After the static clutter suppression, the residual signal matrix $\mathscr{R}$ mainly contains vibration reflections in slow-time *column*s, while the corresponding distances are indicated by fast-time bins. However, as $\mathscr{R}$ is still pretty noisy, we cannot use a plain threshold to differentiate the vibrating targets among the bins. Because our objective is selecting the candidate range bins containing vibration of high SNRs, we observe that, for bins potentially containing vibrations, there exists a certain concentration in the frequency spectrum.[1] For instance, human breaths have a dominant frequency at around 0.2 Hz. Therefore, we perform FFT along each column of $\mathscr{R}$ to obtain $\hat{\mathscr{R}}$, and we use Herfindahl-Hirschman Index (HHI) [42] to calculate the concentration level of those spectra as follows:

$$\text{HHI}(i) = \sum_{j=1}^{K}\left(\frac{\hat{\mathscr{R}}^2(i,j)}{\sum_{j=1}^{K}\hat{\mathscr{R}}^2(i,j)}\right)^2 \tag{10}$$

We select the range bins whose HHIs are higher than a threshold as the candidates containing vibration targets. In other words, we stick to the bin-based sampling to be fair to all RF devices, although some have shown to demand more sophisticated sampling methods in Sec. III-E.

c) Extracting Vibration Signals: For an arbitrary vibration target, we cannot assume a prior knowledge on its frequency range. In other words, we need to figure out which frequency band contains the concerned vibration before applying a bandpass filter. For this purpose, we apply autocorrelation to the columns in $\mathscr{R}$ whose corresponding bins have been selected by the previous *target differentiation* module. As autocorrelation can "highlight" the periodic components in a given signal, it enables us to identify the frequency range without any prior knowledge, which then allows us to finally use a 128th-order bandpass FIR filter to extract the vibration signal. In reality, the vibration signals of a concerned target may be involved in several consecutive bins (depending on the sensing bandwidth). Because the vibration signals contained in all these bins are essentially the same, we combine them to improve the signal SNR.

B. Vibration Sensing Algorithms

Two main approaches leveraging the slow-time dimension for vibration frequency sensing exist, namely *time domain* and *frequency domain*. The time domain approach actually adopts a peak finding algorithm inspired by Eqn. (2): since RF signals vary according to $\Delta d(t)$ induced by vibration, this approach counts the number of peaks within a fixed time window to deduce the vibration frequency. The frequency domain approach applies FFT or STFT to transform input data into frequency domain; it finds the frequency index with the maximum power to indicate the vibration frequency. As suggested by Eqn. (2), $\Delta d(t)$ has a strong frequency component determined by f^{v}, and this component certainly has higher power than other non-periodic components in frequency domain. Whereas the above two approaches rely only on signal amplitude, the received signals are actually in complex form, i.e., containing *phase* information. As Eqn. (1) indicates a linear relation between $\Delta d(t)$ and the baseband phase $2\pi f_c \tau$, this time-varying phase information may allow a full-fledged vibration sensing: not just frequency, but amplitude and hence the waveform. Nonetheless, we shall emphasize on comparing these three approaches for **vibration frequency sensing** in the following, as the sensing ability for vibration amplitude is clearly determined by f_c.

V. Evaluations and Comparisons

In this section, we evaluated five different RF technologies (see Table I) for sensing vibrations. Although Wi-Fi performs

[1] According to Sec. III-B, the concept of range bin may not work for Wi-Fi due to its limited bandwidth, yet we still treat each OFDM subcarrier as a bin for the sake of unified treatment in our study.

reasonably well in the literature [22], [38], [25], [29], [30], our experiments show otherwise. This could be partially caused by our low-complexity processing pipeline. However, these fair comparisons also demonstrate that COTS radios dedicated to sensing can achieve a good performance even with this very basic processing method.

A. Experiment Setup

For micro-benchmarks in Sec. V-B, we evaluate RF technologies in controlled experiments. In particular, we build a *rotary* using LEGO Education EV3; it is programmed to rotate at a certain frequency ranging from 0 to 100 rpm (revolutions per minute), and with a radius from 1 to 15 cm. The distance between the RF device and vibration target is 1.5 m unless otherwise stated, and we use an optical laser sensor [12] to obtain the ground truth. For application case studies in Sec. V-D, the experiment settings are similar, but we adopt a NEULOG respiration monitor belt logger [43] and the Heal Force Prince-180B monitor [44] to obtain the ground truth of respiration and heartbeat respectively. Among three sensing algorithms explained in Sec. IV-B, our comparison study (left to a full report due to page limit) shows that the frequency domain approach is the most robust method, so we shall stick to this algorithm in the following.

B. Micro-Benchmarks

As shown in Fig. 4, we place the rotary so that radio waves propagate vertically to its rotation plane. As our sensing target is the vibration frequency, we use the *absolute error*, i.e., the absolute difference between the estimated frequency and the ground truth, as the performance metric. In the following, we check this metric against various properties of the rotary, including frequency, radius, and orientation. We also evaluate the impact of the environment factors, such as sensing distance, blockage by different materials, and the number of targets.

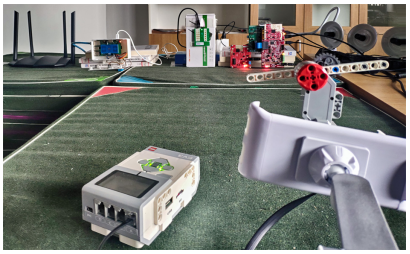

Fig. 4: Experiment setting.

1) Frequency: We vary the rotation speed to emulate the changes in vibration frequency, and we choose to report two cases in Fig. 5. The results show that most devices perform well (median errors below 1 rpm) under 84.5 rpm except Wi-Fi, but only IR-UWB still works under 7.6 rpm. The latter can be an artifact caused by our simple sampling/processing pipeline: it cannot well handle mmWave radios' high sensitivity to the rotary's very noisy motion at a very low speed. Therefore, we fix the rotation speed to 84.5 rpm hereafter.

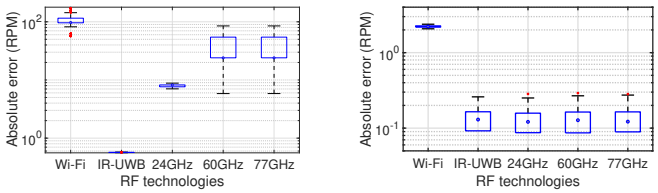

(a) 7.6 rpm. (b) 84.5 rpm.

Fig. 5: Impact of vibration frequency.

2) Vibration Amplitude: The vibration amplitude, emulated by the rotary radius, is set to 5 and 15 cm in this experiment. The results shown in Fig. 6 reveal that amplitude virtually has no impact on the sensing performance, seemingly contradicting the intuition that a larger amplitude should result in a higher v-SNR defined in Eqn. (8) hence a better performance. However, the sensitivity to vibration frequency can be sufficient even with a minor amplitude, further corroborated by later studies on vital sign monitoring. As a side note, the slight abnormal behavior of 60 GHz mmWave radio is likely to be caused by a minor defect of the product, since this system error appears in several other experiments. We also calculate the average v-SNRs under three vibration amplitudes for different devices and report the results in Fig. 7. Since we use the bin-based sampling introduced in Sec. III-E for fair comparison, a too large (15 cm) amplitude can make the sampling miss the vibration trace, leading to low v-SNRs.

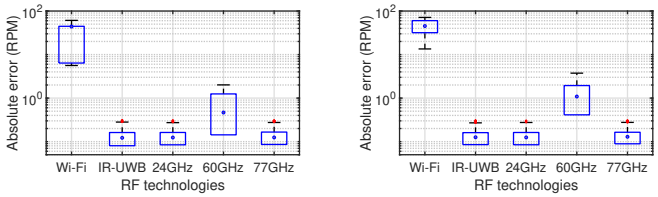

(a) 5 cm vibration amplitude. (b) 15 cm vibration amplitude.

Fig. 6: Impact of vibration amplitude.

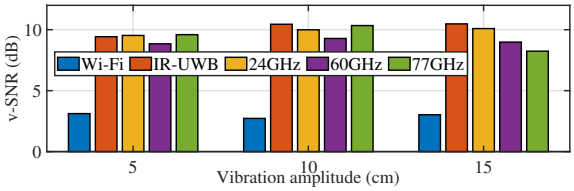

Fig. 7: v-SNR of different vibration amplitude.

3) Orientation: The rotary orientation can change the effective area of the reflection surface, which in turn affect the vibration sensing performance. To validate this intuition, we conduct experiments at different orientations and the results are shown in Fig. 8. It is observable that the accuracy of all RF devices slightly decrease when the orientation changes from 30° to 60°. The extreme case with 90° orientation actually converts rotation to reciprocation, which can still be sensed as vibration, so the impact of orientation is not as strong as for the case of vital sign monitoring.

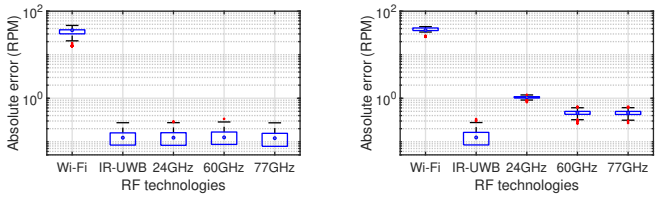

(a) Orientation of 30°. (b) Orientation of 60°.

Fig. 8: Impact of rotary orientation.

4) Distance: We place the rotary at 1, 2, and 3 m distances from the sensing devices to explore the impact of distance, and the results are reported in Fig. 9. Not surprisingly, the performance of all RF devices degrade in performance as the distance increases, yet the impact is really minor. In order to better understand how distance affects the sensing performance, we refer to the v-SNR metric again. As shown in Fig. 10, the v-SNRs of all RF devices decrease monotonously from 1 to 3 m, but that of IR-UWB appears to be less sensitive to distance, and that of 24 GHz (with 250 MHz bandwidth) degrades faster than others. While the case of IR-UWB can be explained by its moderate bandwidth, that of 24 GHz may be caused by inevitable multipath interference unable to be filtered out by its insufficient range resolution.

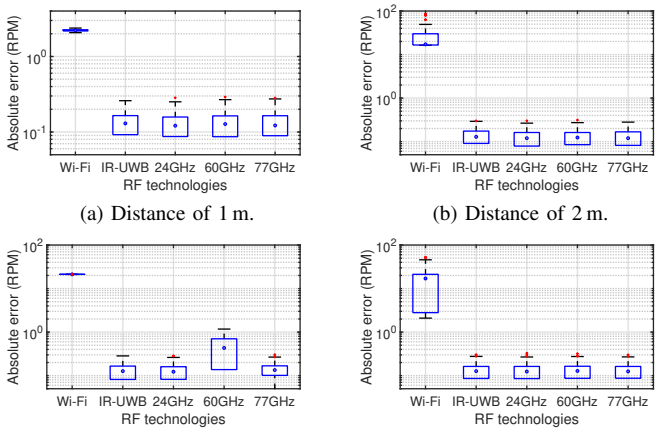

(a) Distance of 1 m. (b) Distance of 2 m.

(c) Distance of 3 m. (d) Overall Error.

Fig. 9: Impact of sensing distance.

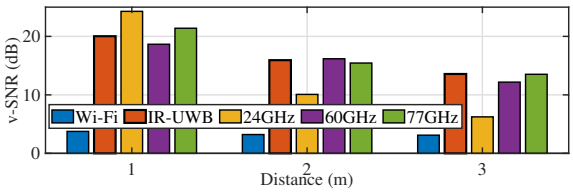

Fig. 10: v-SNR at different distances

5) Blocking Material: To evaluate the environment impact on different RF technologies, we block the rotary using 4 different materials: brick, cotton, wood, and glass, and we report the results in Fig. 11. We can see all five RF devices can penetrate cotton and glass, while 60/77 GHz mmWave radiations fail to penetrate brick and perform badly for wood.

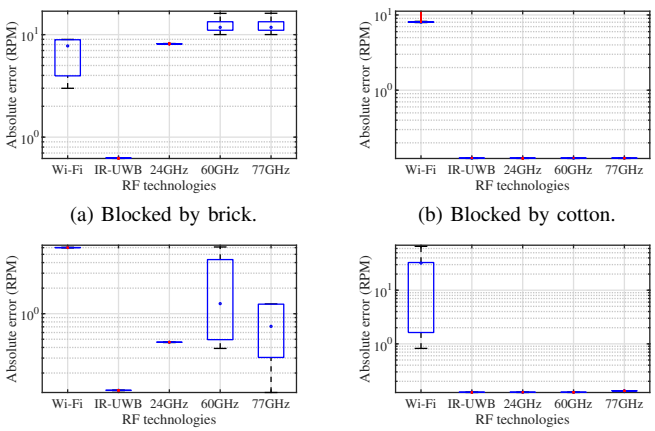

(a) Blocked by brick. (b) Blocked by cotton.

(c) Blocked by wood. (d) Blocked by glass.

Fig. 11: Impact of different blocking materials.

As 24 GHz mmWave radio has a slightly longer wavelength, it achieves an better accuracy than the other mmWave radios. We suspect the reason is that some crevices exist in the brick wall that we temporarily build, and the 24 GHz radio, with stronger power (than IR-UWB) and diffraction capability (than 60/77 GHz counterparts), successfully penetrates the brick wall. We also observe unreasonably high bias and low variance for the measurements of 60/77 GHz radios in Fig. 11(a). In fact, no effective vibration can be detected by 60/77 GHz radios, and the false frequencies are caused by the boundary effect of the band-pass filter. Such artifacts can be readily removed by employing another sensing algorithm (e.g., time-domain method) explained in Sec. IV-B.

6) Number of Targets: The number of co-existing targets is another factor to be considered, as realistic scenarios may have multiple vibration targets to potentially interfere each other in measurements. We put the 3 vibration targets in front of sensing devices with mutual distance being 1 m, 1.7 m and 2 m to measure their vibration. As shown in Fig. 12, only marginally affect the estimation accuracy for IR-UWB and two mmWave (60 GHz and 77 GHz) radios, as their wide bandwidths allow them to differentiate these targets, rather than mixing their vibrations together as with Wi-Fi.

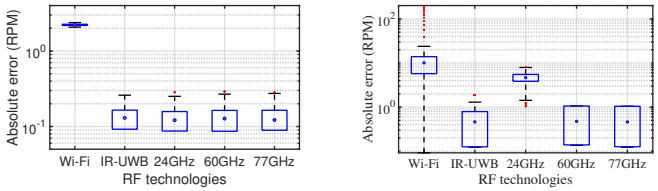

(a) 1 target in the space. (b) 3 targets in the space.

Fig. 12: Impact of the numbers of targets.

C. Case Study 1: Machinery Vibration

A key issue of rotation machinery that can be indicated by vibration is eccentric unbalance. While we focus on vibration frequency sensing earlier, we hereby verify another ability of RF sensing for **variation of vibration amplitude**; this value

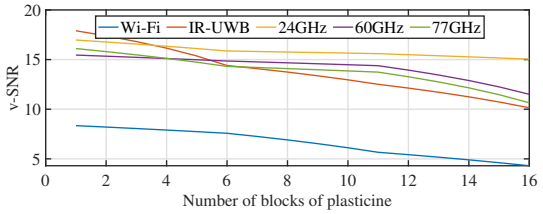

Fig. 13: Sensitivities of v-SNR to eccentric unbalance.

indicates the extent of eccentric unbalance of a rotating part. To emulate a varying level of unbalance, we gradually add small blocks of plasticine on one fan blade. This increasing unbalance causes the spectrum around the rotation frequency to "spread out", which in turn leads to a monotonic reduction in the peak power. Theoretically, we may detect this peak power reduction by monitoring the v-SNR profile. The experiment results shown in Fig. 13 exactly corroborate this conjecture. Though all 5 RF devices can detect this minor variation, IR-UWB appears to be more sensitive and hence may potentially achieve a higher detection accuracy. We leave a full-fledged quantitative study in our full report.

D. Case Study 2: Vital Signs

Now we apply RF vibration sensing to human vital sign monitoring. Different from the studies in [22], we perform the measurements under daily life and work conditions, and we monitor both respiration rate and heartbeat rate.

1) Distance: A key factor affecting the vital sign estimation error is the distance between the human body and sensing devices. Corroborating the results in Sec. V-B4, the performance of vital sign monitoring also slightly degrade with the increase in sensing distance, as shown in Fig. 14, which is can again be explained by the v-SNR over distance profile shown in Fig. 15. It is curious to observe that the 24 GHz obtains the highest v-SNRs. The reason is twofold: i) The human body is much larger than the rotary, so the total signal strength within a wider range can be higher, and ii) according to Sec. III-E, the bin-based sampling of 24 GHz is similar to

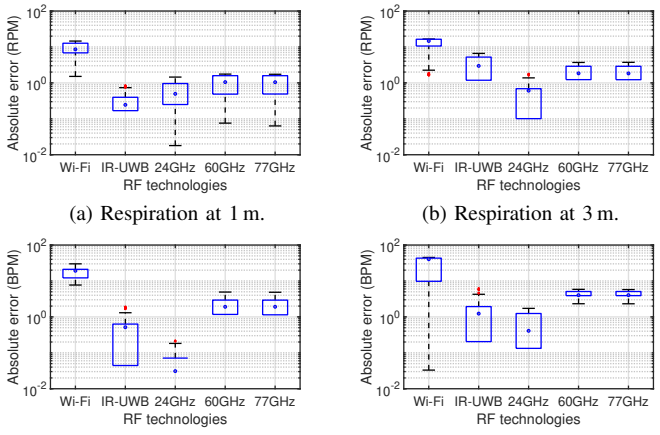

(a) Respiration at 1 m. (b) Respiration at 3 m.

(c) Heartbeat at 1 m. (d) Heartbeat at 3 m.

Fig. 14: Impact of distance on vital sign estimations.

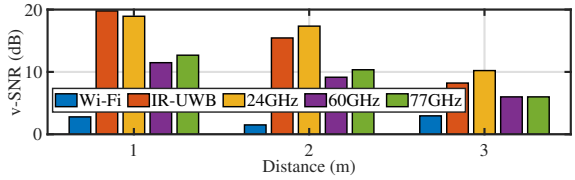

Fig. 15: v-SNR at different distances

directly merging multiple range bins under a wider bandwidth, potentially leading to a higher v-SNR.

2) Orientation: The orientation of the human body also affects the vital sign monitoring; here 0° orientation means radio waves propagate vertically to human face. In Fig. 16, we can see that the errors of all RF devices go up when the orientation changes from 30° to 60°. The reason is that the movement of human body (driven by either respiration or heartbeat) can be modeled as reciprocation, whose modulation effect on radio waves is more sensitive to orientation than rotation (see Sec. V-B3). According to Fig. 16, the estimation accuracy of heartbeat sensing is significantly better than respiration sensing. A possible explanation is that, whereas respiration most causes chest/abdomen reciprocation, heartbeat affects many parts on human body, including common carotid arteries via the neck.

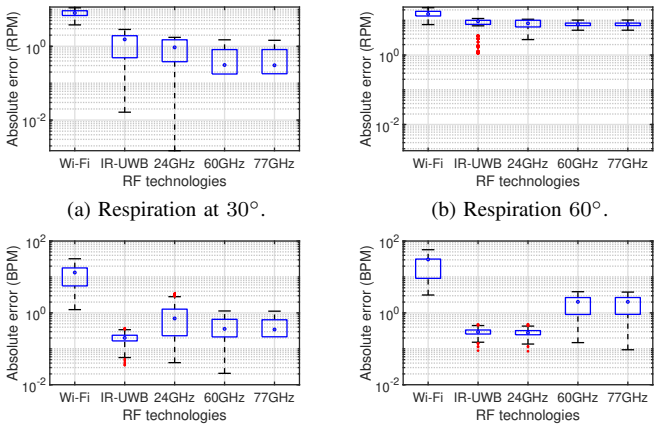

(a) Respiration at 30°. (b) Respiration 60°.

(c) Heartbeat at 30°. (d) Heartbeat at 60°.

Fig. 16: Impact of human body orientation.

3) Number of Human Subjects: It is possible that multiple people need to be put under monitoring, so we hereby evaluate the capability of different RF technologies in handling multi-person vital sign monitoring. According to Fig. 17, the performance degrades for all 5 RF devices when the number of monitored people increases from 1 to 3, yet IR-UWB largely maintains a competent performance. In fact, we can only retrieve one reading from Wi-Fi, as its narrow bandwidth cannot differentiate targets. The relative unsatisfactory performance of mmWave radios may be caused by our simple processing pipeline that neglects the opportunity of spatial-temporal joint estimation offered by their antenna arrays, but our simple method is generally sufficient.

4) Blocking Material: Similar to Sec. V-B5, we evaluate the effects of different blocking materials on vital sign estimation.

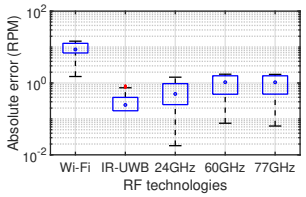

(a) Respiratory rate with 1 people.

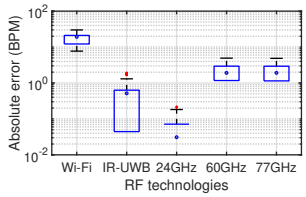

(b) Heartbeat rate with 1 people.

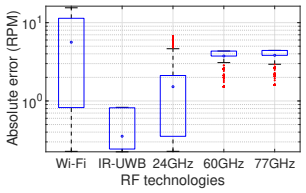

(c) Respiratory rate with 3 people.

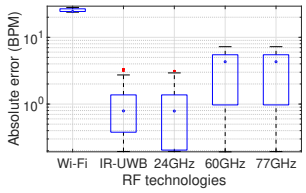

(d) Heartbeat rate with 3 people.

Fig. 17: Impact of number of human subjects.

Due to page limit, we omit two materials (i.e., brick and wood) as they almost block the mmWave signals completely and bring no insight into our evaluation. We choose cotton and glass to block the human body, and report the vital sign estimation performance in Fig. 18. We again reach the same conclusion that IR-UWB and 24 GHz mmWave radio have the most robust penetration performance.

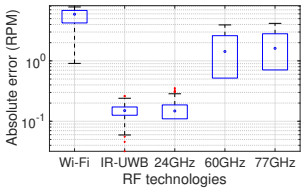

(a) Blocked by cotton (R).

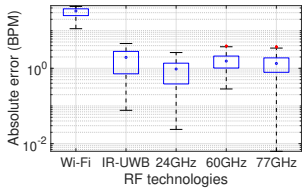

(b) Blocked by cotton (H).

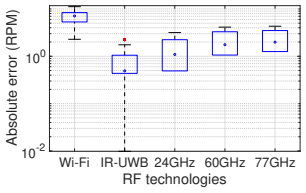

(c) Blocked by glass (R).

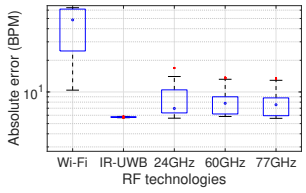

(d) Blocked by glass (H).

Fig. 18: Impact of different blocking materials on vital sign estimation (R - respiration, H - heartbeat).

5) Window Size: We also evaluate the effects of different window sizes on vital sign estimation. The results shown in Fig. 19 have omitted heartbeat results since they are similar to respiration. An interesting insight here is when the window size increases, the estimation results get more stable: the variances of IR-UWB and 60/77 GHz mmWave radios become smaller with a larger window size. Another effect of a larger window size is increased accuracy, as demonstrated by the 24 GHz mmWave radio, whose estimation error is greatly reduced by using a larger window size. Nonetheless, a larger window also leads to a longer estimation latency.

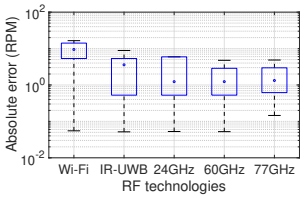

(a) Window size of 15 s.

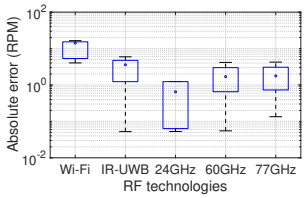

(b) Window size of 35 s.

Fig. 19: Impact of window size on resp. rate estimation.

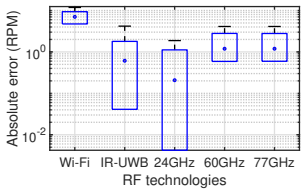

(a) Typing on keyboard.

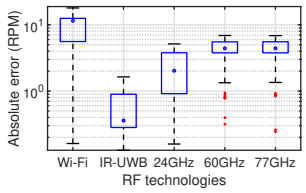

(b) Standing Up.

Fig. 20: Impact of body movement on resp. rate estimation.

6) Body Movement: The existence of human body movement may affect the accuracy of vital sign estimations, but this impact is overstated in [22]: all measurements are trashed upon a detection of body movement. Our results in Fig. 20 demonstrate that respiratory rate estimations are not seriously affected by either (quasi-)periodic movements (typing on keyboards) or sudden movements (standing up), although sudden movements do cause certain performance degradation, especially for mmWave radios. We omit heartbeat results again due to their similarity to respiration.

VI. Conclusion

In this paper, we have conducted the first systematic comparative study on COTS-RF technologies, concerning their ability in sensing vibration. Our study involves five typical COTS-RF devices, namely Wi-Fi, IR-UWB, and 24/60/77 GHz mmWave radios. We first summarize a common signal profile for these devices, then we propose a common metric v-SNR to evaluate sensing quality and a processing pipeline to handle this profile. We take a LEGO rotary to benchmark vibration frequency sensing performance of these RF devices under typical impact factors, before conducting two case studies: i) vibration amplitude sensing for detecting eccentric unbalance in rotation machinery, and ii) human vital sign monitoring. Contradictory to an earlier study [22], we have demonstrated that Wi-Fi has no match to other dedicated sensing devices. In the meantime, we have identified both IR-UWB and 24 GHz mmWave radio as having the best overall performance.

Acknowledgment

This work is supported by Ministry of Education (MOE) Tier 1 Grant No. RG16/22, National Natural Science Foundation of China (Grant No. 62202276), Shandong Science Fund for Excellent Young Scholars (No. 2022HWYQ-038) and National Development and Reform Commission of China (NDRC) under grant "5G Network Enabled Intelligent Medicine and Emergency Rescue System for Giant Cities".

REFERENCES

[1] H. Tongue Benson. *Principles of Vibrations, 2nd Edition*. Oxford University Press, 2002.

[2] Antonio Bayés de Luna, Philippe Coumel, and Jean François Leclercq. Ambulatory Sudden Cardiac Death: Mechanisms of Production of Fatal Arrhythmia on the Basis of Data from 157 Cases. *American Heart Journal*, 117(1):151–159, 1989.

[3] J. Anthony Gomes, Dimitrios Alexopoulos, Stephen L. Winters, Pramod Deshmukh, Valentin Fuster, and Kiung Suh. The Role of Silent Ischemia, the Arrhythmic Substrate and the Short-Long Sequence in the Genesis of Sudden Cardiac Death. *Journal of the American College of Cardiology*, 14(7):1618–1625, 1989.

[4] Chin-Hsiung Loh, Kenneth J Loh, Yuan-Sen Yang, Wan-Ying Hsiung, and Yu-Ting Huang. Vibration-based System Identification of Wind Turbine System. *Structural Control and Health Monitoring*, 24(3):1876–1877, 2017.

[5] Nam Bui, Nhat Pham, Jessica Jacqueline Barnitz, Zhanan Zou, Phuc Nguyen, Hoang Truong, Taeho Kim, Nicholas Farrow, Anh Nguyen, Jianliang Xiao, et al. eBP: A Wearable System For Frequent and Comfortable Blood Pressure Monitoring From User's Ear. In *Proc. of the 25th ACM MobiCom*, pages 1–17, 2019.

[6] Nirupam Roy, Mahanth Gowda, and Romit Roy Choudhury. Ripple: Communicating through Physical Vibration. In *Proc. of the 12th USENIX NSDI*, pages 265–278, 2015.

[7] Phuc Nguyen, Xinyu Zhang, Ann Halbower, and Tam Vu. Continuous and Fine-Grained Breathing Volume Monitoring from Afar Using Wireless Signals. In *Proc. of the 35th IEEE INFOCOM*, 2016.

[8] Chengkun Jiang, Junchen Guo, Yuan He, Meng Jin, Shuai Li, and Yunhao Liu. mmVib: Micrometer-Level Vibration Measurement with mmWave. In *Proc. of the 26th ACM Mobicom*. ACM, 2020.

[9] Zhe Chen, Tianyue Zheng, Chao Cai, and Jun Luo. MoVi-Fi: Motion-robust Vital Signs Waveform Recovery via Deep Interpreted RF Sensing. In *Proc. of the 27th ACM MobiCom*, pages 392—-405, 2021.

[10] Shujie Zhang, Tianyue Zheng, Zhe Chen, and Jun Luo. Can We Obtain Fine-grained Heartbeat Waveform via Contact-free RF-sensing? In *Prof. of the 41st IEEE INFOCOM*, pages 1759–1768, 2022.

[11] Anhui Ronds Science & Technology Incorporated Company. Wireless Vibration Monitoring - Wireless Vibration Sensor. http://www.ronds.com/, 2022. Accessed: 2022-07-21.

[12] Fluke Corporation. Fluke 820-2 LED Stroboscope. https://www.fluke.com/en-sg/product/mechanical-maintenance/vibration-analysis/fluke-820-2, 2019. Accessed: 2022-07-21.

[13] Novelda AS. Single-chip radar sensors with sub-mm resolution - xethru. https://www.xethru.com/, 2017. Accessed: 2022-07-03.

[14] Infineon Technologies AG. Industrial Radar Sensing. https://www.infineon.com/dgdl/Infineon-Position2Go_development_kit-PB-v01_00-EN.pdf?fileId=5546d46267c74c9a0167cabc70cd0120, 2018. Accessed: 2022-07-23.

[15] Texas Instruments Incorporated. IWR6843 Intelligent mmWave Overhead Detection Sensor (ODS) Antenna Plug-in Module. https://www.ti.com/tool/IWR6843ISK-ODS, 2020. Accessed: 2022-07-23.

[16] Texas Instruments Incorporated. IWR1443BOOST Evaluation Module mmWave Sensing Solution. https://www.ti.com/lit/ug/swru518d/swru518d.pdf, 2020. Accessed: 2022-07-23.

[17] Daniel Halperin, Wenjun Hu, Anmol Sheth, and David Wetherall. Tool Release: Gathering 802.11n Traces with Channel State Information. *ACM SIGCOMM CCR*, 41(1):53, Jan. 2011.

[18] Tianyue Zheng, Zhe Chen, Chao Cai, Jun Luo, and Xu Zhang. V2iFi: in-Vehicle Vital Sign Monitoring via Compact RF Sensing. In *Proc. of the 20th ACM UbiComp*, pages 70:1–27, 2020.

[19] Tianyue Zheng, Zhe Chen, Shujie Zhang, Chao Cai, and Jun Luo. MoRe-Fi: Motion-robust and Fine-grained Respiration Monitoring via Deep-Learning UWB Radar. In *Proc. of the 19th ACM SenSys*, pages 111–124, 2021.

[20] Chenhan Xu, Zhengxiong Li, Hanbin Zhang, Aditya Singh Rathore, Huining Li, Chen Song, Kun Wang, and Wenyao Xu. WaveEar: Exploring a mmWave-based Noise-Resistant Speech Sensing for Voice-User Interface. In *Proc. of the 17th ACM MobiSys*, pages 14–26, 2019.

[21] Fuming Chen, Sheng Li, Yang Zhang, and Jianqi Wang. Detection of the Vibration Signal from Human Vocal Folds Using a 94-GHz Millimeter-Wave Radar. *Sensors*, 17(3):543, 2017.

[22] Peter Hillyard, Anh Luong, Alemayehu Solomon Abrar, Neal Patwari, Krishna Sundar, Robert Farney, Jason Burch, Christina Porucznik, and Sarah Hatch Pollard. Experience: Cross-Technology Radio Respiratory Monitoring Performance Study. In *Proc. of the 24th ACM MobiCom*, pages 487–496, 2018.

[23] Jyun-Long Chen, Tien-Cheng Tseng, Yu-Yi Cheng, Kuang-I Chang, and Jwu-Sheng Hu. Using UWB Sensor for Delta Robot Vibration Detection. In *2013 IEEE/RSJ International Conference on Intelligent Robots and Systems*, pages 419–423. IEEE, 2013.

[24] Te-Yu J Kao, Yan Yan, Tze-Min Shen, Austin Ying-Kuang Chen, and Jenshan Lin. Design and Analysis of a 60-GHz CMOS Doppler Micro-Radar System-in-Package for Vital-Sign and Vibration Detection. *IEEE Trans on Microwave Theory and Techniques*, 61(4):1649–1659, 2013.

[25] Teng Wei, Shu Wang, Anfu Zhou, and Xinyu Zhang. Acoustic Eavesdropping through Wireless Vibrometry. In *Proc. of the 21st ACM MobiCom*, pages 130–141, 2015.

[26] Yu Rong, Sharanya Srinivas, Adarsh Venkataramani, and Daniel W Bliss. UWB Radar Vibrometry: An RF Microphone. In *Proc. of the 53rd Asilomar CSSC*, pages 1066–1070, 2019.

[27] Xujun Ma, Yiyang Wang, Wenlian Song, Xiaohu You, Jenshan Lin, and Lianming Li. A 100-GHz Double-Sideband Low-IF CW Doppler Radar in 65-nm CMOS for Mechanical Vibration and Biological Vital Sign Detections. In *2019 IEEE MTT-S International Microwave Symposium (IMS)*, pages 136–139. IEEE, 2019.

[28] Christopher T Rodenbeck, Joshua B Beun, Raghu G Raj, and Ronald D Lipps. Vibrometry and Sound Reproduction of Acoustic Sources on Moving Platforms Using Millimeter Wave Pulse-Doppler Radar. *IEEE Access*, 8:27676–27686, 2020.

[29] Heba Abdelnasser, Khaled A. Harras, and Moustafa Youssef. UbiBreathe: A Ubiquitous Non-Invasive WiFi-based Breathing Estimator. In *Proc. of the 16th ACM MobiHoc*, 2015.

[30] Xuefeng Liu, Jiannong Cao, Shaojie Tang, Jiaqi Wen, and Peng Guo. Contactless Respiration Monitoring via Off-the-Shelf WiFi Devices. *IEEE Transactions on Mobile Computing*, 15(10):2466–2479, 2015.

[31] Jian Liu, Yan Wang, Yingying Chen, Jie Yang, Xu Chen, and Jerry Cheng. Tracking Vital Signs During Sleep Leveraging Off-the-Shelf WiFi. In *Proc. of the 16th ACM MobiHoc*, pages 267–276, 2015.

[32] Youwei Zeng, Enze Yi, Dan Wu, Ruiyang Gao, and Daqing Zhang. A Full Human Respiration Detection System using Commodity Wi-Fi Devices. In *Proc. of the 18th ACM UbiComp*, pages 480–483, 2018.

[33] Timo Lauteslager, Mathias Tømmer, Tor Sverre Lande, and Timothy G Constandinou. Coherent UWB Radar-on-Chip for In-Body Measurement of Cardiovascular Dynamics. *IEEE Transactions on Biomedical Circuits and Systems*, 13(5):814–824, 2019.

[34] Fengyu Wang, Feng Zhang, Chenshu Wu, Beibei Wang, and K.J. Ray Liu. ViMo: Multi-person Vital Sign Monitoring using Commodity Millimeter Wave Radio. *IEEE Internet of Things Journal*, 2020.

[35] Sang-Gyu Kim, Gi-Ho Yun, and Jong-Gwan Yook. Wireless RF Vital Signal Sensor Using Autoregressive Spectral Estimation Method. *IEEE Antennas and Wireless Propagation Letters*, 11:535–538, 2012.

[36] Elliott Schires, Pantelis Georgiou, and Tor Sverre Lande. Vital Sign Monitoring through the Back Using an UWB Impulse Radar with Body Coupled Antennas. *IEEE Transactions on Biomedical Circuits and Systems*, 12(2):292–302, 2018.

[37] Wenfeng Yin, Xiuzhu Yang, Lin Zhang, and Eiji Oki. ECG Monitoring System Integrated with IR-UWB Radar based on CNN. *IEEE Access*, 4:6344–6351, 2016.

[38] Wenjia Jia, Hongjian Peng, Na Ruan, Zhiping Tang, and Wei Zhao. WiFind: Driver Fatigue Detection with Fine-Grained Wi-Fi Signal Features. *IEEE Transactions on Big Data*, pages 1–14, 2018.

[39] David Tse and Pramod Viswanath. *Fundamentals of Wireless Communication*. Cambridge University Press, USA, 2005.

[40] Victor C Chen, Fayin Li, S-S Ho, and Harry Wechsler. Micro-Doppler Effect in Radar: Phenomenon, Model, and Simulation Study. *IEEE Transactions on Aerospace and Electronic Systems*, 42(1):2–21, 2006.

[41] Bassem R. Mahafza. *Radar Systems Analysis and Design Using MATLAB*. CRC press, 2002.

[42] Charles R Laine. The Herfindahl-Hirschman Index: A Concentration Measure Taking the Consumer's Point of View. *The Antitrust Bulletin*, 40(2):423–432, 1995.

[43] NeuLog. Respiration Monitor Belt Logger Sensor NUL-236. https://neulog.com/respiration-monitor-belt/, 2017. Accessed: 2022-07-21.

[44] Heal Force. Easy ECG Monitor – Prince-180B (B0). http://www.healforce.com, 2019. Accessed: 2022-07-28.